



Performance Evaluation of Small Scale Air-Conditioning System Using R22 and Alternative Refrigerants

Prof. Dr. Khalid Ahmed Al-Joudi
Department of Mechanical Engineering
College of Engineering
Baghdad University
Email:Khalid47joudi@yahoo.com

Asst. Lect. Qusay Rasheed Abd Al-Amir
Department of Mechanical Engineering
College of Engineering
Baghdad University
Email:Qusay1972@gmail.com

ABSTRACT:

A mathematical model has been formulated to predict the influence of high outdoor air temperature on the performance of small scale air - conditioning system using R22 and alternative refrigerants R290, R407C, R410A. All refrigerants were investigated in the cooling mode operation. The mathematical model results have been validated with experimental data extracted from split type air conditioner of 2 TR capacity. This entailed the construction of an experimental test rig which consists of four main parts. They are, the refrigeration system, psychrometric test facility, measuring instrumentation, and auxiliary systems. The conditioned air was maintained at 25 °C dry bulb and 19 °C wet bulb for all tests. The outdoor ambient air temperature was varied from 35 °C to 55 °C in 5 °C increments. The study showed that R290 is the better replacement for R22 when the air conditioning system works under high ambient temperature. It has better performance as a drop in refrigerant. R407C has the closest performance to R22, followed by R410A.

KEYWORDS: Numerical and experimental refrigeration cycle performance; Mathematical model; Small air conditioner; Alternative refrigerants at high ambient temperature.

تقييم أداء منظومة تكييف هواء صغيرة الحجم باستخدام R22 وموائع بديلة

م.م. قصي رشيد عبد الامير
قسم الهندسة الميكانيكية
جامعة بابل

أ.د. خالد أحمد الجودي
قسم الهندسة الميكانيكية
جامعة بغداد

الخلاصة :

تم بناء نموذج رياضي يحاكي تأثير ارتفاع درجة حرارة الهواء الخارجي على الأداء التشغيلي لمكيف هواء صغير السعة يعمل بمائع التثليج R22 و بدائله R290, R407C, R410A و بطور التبريد. قورنت نتائج النموذج رياضي لهذه الدراسة بنتائج عملية من مكيف هواء مُنفصل سعة 2 طن تبريد. استلزم ذلك بناء جهاز اختبار تجريبي يتكون من أربعة أجزاء وهي نظام التثليج وحجرات الاختبار البيئية ومعدات القياس وأجهزة السيطرة على درجات الحرارة. تم تثبيت درجة حرارة الهواء الداخلية عند 25 °م بصللة جافة و 19 °م بصللة رطبة. بينما تغيرت درجات حرارة الهواء الخارجية من 35 °م إلى 55 °م بزيادات مقدارها 5 °م كل مرة. أثبتت الدراسة أنّ مائع التثليج R290 هو البديل الأفضل إلى مائع التثليج R22 عندما يعمل نظام التكييف تحت درجات حرارة بيئية عالية. كان مائع التثليج R407C اقرب أداءاً إلى المائع R22 و يأتي بعده R410A.

الكلمات الرئيسية: دراسة عددية و تجريبية لدورة التثليج، نموذج رياضي، مكيف هواء صغير السعة ، موائع بديلة عند ظروف بيئية قاسية.

1. INTRODUCTION

Many mathematical models have been proposed in the past for modeling refrigeration systems. These models can be classified as steady state and transient simulations. Steady state simulations are commonly used for performance prediction and product design. In other words, vapor compression systems are rated and designed using steady state performance evaluations. Rice et al. (1981) used steady state simulation to explore optimization of conventional air-to-air heat pumps. The model was used to calculate the maximum coefficient of performance that can be attained, both with components that are presently available and with improved ones, for a range of heat exchanger sizes. Another model to predict the steady state performance of an air to air heat pump model was developed by Fisher and Rice (1983). This model is known as the ORNL heat pump model. The model was written using Fortran-IV computer program. In medium temperature refrigeration systems, Spatz et al. (2004) evaluated the performance of R22 with its potential alternatives of R410A, R404A, and R290. The results show that R410A is an efficient and environmentally acceptable option to replace R22 in medium temperature applications. According to Cabello et al. (2005), a simplified steady-state model of a single stage vapor compression plant was presented based on empirical and parametrical correlations. This model has been validated by experimental data obtained from a test bench using refrigerants R134a, R407C and R22. In 2007, Techarungpaisan et al. proposed a steady state simulation model to predict the performance of a small split type air conditioner with an integrated water heater. This model was also used to predict system parameters of interest such as hot water temperature, condenser exit air temperature, evaporator exit air temperature, mass flow rate of refrigerant, heat rejection in condenser and cooling capacity of the system.

In addition to the above, other models have been proposed as simulation tools for vapor compression refrigeration cycles such as VapCyc, and CYCLE-D. Richardson et al. (2004) presented VapCyc, which is a steady state simulation tool for the modeling and optimization of vapor

compression refrigeration system and its components. The simulation limits the user to the basic four component system. The simulation consists of a set of independent variables, such as system charge, component model numbers and component independent variables, and results in a set of dependent system variables, such as COP, capacity, weight and volume. Another simulation tool called CYCLE-D offered by the National Institute of Standards and Technology (NIST) for the theoretical analysis of a vapor compression system was used by Domanski et al. (2005). The goal of their results was to assess the impact of the evaporator performance on the COP for different refrigerants.

In this model, a comparative performance of R22 and its alternatives R290, R407C and R410A were determined theoretically in an attempt to examine the possibility of substituting R22 in residential air conditioners used in summer hot arid climate.

2-MATHEMATICAL MODELING

The refrigeration cycle consists of four major components; a rotary compressor running at constant speed, a finned-tube condenser coil, an evaporator coil, and capillary tubes. These components are connected by pipes which may be surrounded by insulation. Other components such as a filter-driers and an accumulator are neglected in this analysis due to their relatively small influence on the performance of the system (Jin and Spitler 2002). These components form a complete refrigeration cycle. In order to simulate the cycle, all models are interconnected with each other to form the complete model. The thermodynamic properties of R22 and the alternative refrigerants are calculated using the Engineering Equation Solver (EES) software (Klein 2006). These properties are calculated from the equation of state (EOS). The cycle presented in **Fig.1** is representative of a single-stage, vapor compression refrigeration cycle.

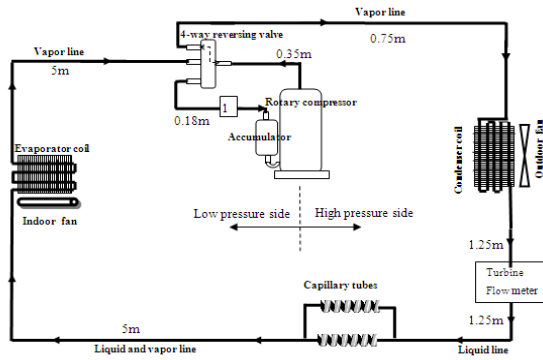


Fig.1 Schematic diagram of a split type A/C system

The pressure-enthalpy diagram for an actual system with state points is shown in Fig.2. It is noted that due to pressure drop across both the suction line and discharge line, the suction pressure (P_1) is slightly lower than the evaporator pressure (P_e), while the discharge pressure (P_2) is higher than the condenser pressure (P_c).

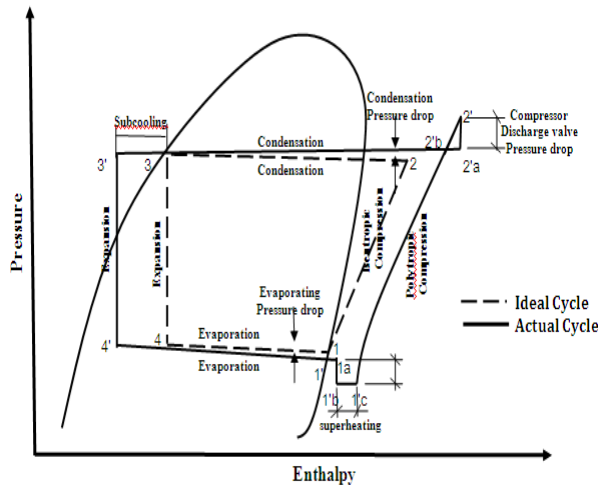


Fig.2 Ideal and real refrigeration cycles.

2.1 Modeling of Rotary Compressors

The following assumptions for the rotary compressor are made:

1. Compressor operates at steady state conditions.
2. Compression process is assumed polytropic.

3. Changes in kinetic and potential energies are negligible.
4. Compressor motor and mechanical efficiency are taken to be 78% and 92.5%, respectively (Wakabayashi et al. 1982).
5. The temperature of the gas along with the shell is constant.
6. Pressure drop across the discharge valve is isenthalpic.
7. The flow through the compressor is homogeneous and one dimensional.
8. The oil effects on the refrigerant properties are neglected.

In an actual compression process, the entropy increases as the irreversibilities of the process increase. Therefore, the compression process in the compressor is normally polytropic. The power of compressor is calculated according to the following equation (Winandy 2002):

$$W_{co} = \dot{m}_r \cdot P_1 \cdot v_1 \cdot \frac{n}{n-1} \left[\left(\frac{P_2}{P_1} \right)^{\frac{n-1}{n}} - 1 \right] \quad (1)$$

The theoretical power (w_{co}) can also be calculated in terms of the enthalpy change of refrigerant across the compressor, as follows:

$$W_{co} = \frac{W_{is}}{\eta_{is}} = \dot{m}_r \cdot (H_2 - H_1) \quad (2)$$

The power input to the compressor is determined as;

$$W_i = \frac{W_{co}}{\eta_{ov}} \quad (3)$$

The overall compressor efficiency determines the actual amount of electrical energy required to drive the compressor. This efficiency is calculated by Cho and Jung (2010), and Sakaino et al. (1984) as;

$$\eta_{ov} = \eta_{in} \eta_{me} \eta_{mo} \quad (4)$$

The values of efficiencies η_{mo} and η_{me} are taken as 0.78 and 0.925 respectively (Duprez et. al. 2007),

whereas the indicated efficiency η_i is calculated as (Ding and Zhang 2001):

$$\eta_{in} = \frac{\eta_v}{1 + 1.5 \Delta P_d \left(\frac{P_d}{P_s} \right)^{\frac{1}{n}} \cdot v_s / (H_d - H_s)} \quad (5)$$

The volumetric efficiency η_v of the compressor is calculated from the well known equation:

$$\eta_v = 1 + C - C \left(\frac{P_d}{P_s} \right)^{\frac{1}{n}} \quad (6)$$

It is well known that the rotary compressors have high clearance volumetric efficiencies due to the small clearance volume and corresponding low re-expansion losses of residual gas (Winandy et. al. 2002). In Eq.6, the clearance volume is taken at C=5%. The polytropic index n is given as;

$$n = \frac{\ln \left(\frac{P_d}{P_s} \right)}{\ln \left(\frac{v_s}{v_d} \right)} \quad (7)$$

ΔP_d in Eq.5, is given by Ding and Zhang (2001) as;

$$\Delta P_d = 25(T_d - 273.15)^{-1.01} \cdot 10^{-0.15 \frac{P_d}{P_s}} \quad (8)$$

At steady state, the mass flow rate of refrigerant is assumed to be the same throughout the system and equal to the mass flow rate through the compressor (Blanco et al. 2012). Most compressors operate at a fixed displacement rate. Therefore, the refrigerant mass flow rate will be a function of the suction specific volume as ;

$$\dot{m}_r = \frac{\eta_v \cdot V_d \cdot N}{v_1} \quad (9)$$

The theoretical displacement volume of the compressor (V_d) is calculated from the difference in volume between the roller diameter and cylinder diameter as follows (ASHRAE Handbook 2010);

$$V_d = \frac{\pi \cdot L_{cy} \cdot (D_c^2 - D_r^2)}{4} \quad (10)$$

Where: D_c and D_r are the diameters of the cylinder and rolling piston respectively, and L_{cy} the length or height of the cylinder.

In the compressor, the heat is transferred during the compression cycle due to the temperature difference between the cylinder walls and the refrigerant gas Q_{su} , on one hand, and between the shell and the ambient Q_S on the other hand. It is difficult to study the heat transfer phenomena inside the rotary compressor since it requires knowledge of the internal dimensions and many factors concerning re-expansion of residual gas, mass of return flow, oil and gas leakage and so on. For these reasons, the heat transfer from the shell to the ambient is only considered in this study as in other works (Kim and Bullard (2001), Winkler (2009)). When the compressor shell temperature has reached a steady value, the rate of heat transfer from the refrigerant to the shell is equivalent to the rate of the heat transfer from the shell to the ambient. The heat transfer from the compressor shell can be obtained by applying the first law of thermodynamics across the compressor shell using the following equation for the steady state flow, neglecting the potential and kinetic energies (Duprez et. al., 2007).

$$Q_S = \dot{W}_i - \dot{m}_r (H_d - H_s) \quad (11)$$

2.2 Modeling of Finned Tube Condensers

On the refrigerant side, the condenser is divided into three heat transfer regions, a vapor phase de-superheating region, a two-phase condensing region and a liquid phase subcooling region. Among these three regions, de-superheating and subcooling occupy relatively a small portion. The de-superheating uses about 5 percent of the condensing surface area and subcooling uses 5 to 10 percent (Wang, 2000). The rest of the condenser area undergoes condensation at constant pressure and temperature. **Fig.3** shows a schematic diagram of the heat transfer processes through the condenser.

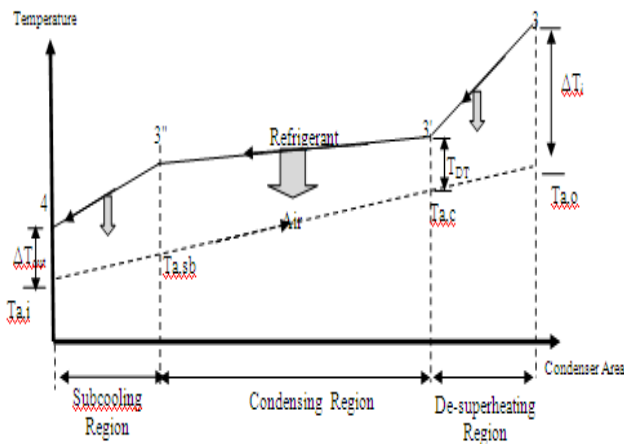


Fig.3 Temperature profile in the condenser

The following assumptions are made in this study;

- 1-One dimensional steady flow,
- 2-Thermodynamic equilibrium between the liquid and vapor (separated flow),
- 3-The condenser coils are assumed to be one dry path.
- 4-In the two phase region, the flow is assumed to be annular flow.
- 5-The air side heat transfer coefficient is constant over the whole condenser.
- 6-The air and refrigerant flow directions are in counter flow configuration.
- 7-The heat transfer and pressure drop effects are considered in the condenser tubes and they are neglected in bends.

The heat rejected from each region can be determined by evaluating the enthalpies at the inlets and outlets.

$$Q_{c,d} = \dot{m}_r (H_3 - H_{3'}) \tag{12}$$

$$Q_{c,t} = \dot{m}_r (H_{3'} - H_{3''}) \tag{13}$$

$$Q_{c,sb} = \dot{m}_r (H_{3''} - H_4) \tag{14}$$

The effectiveness – number of transfer units (ϵ - NTU) method is utilized to find the heat transfer for each region in the heat exchanger, using the temperature difference between the air and refrigerant sides as:

$$Q_{c,d} = \epsilon_d C_{\min} (T_3 - T_{a,c}) \tag{15}$$

$$Q_{c,t} = \epsilon_t C_{\min} (T_{3'} - T_{a,sc}) \tag{16}$$

$$Q_{c,sb} = \epsilon_s C_{\min} (T_{3''} - T_{a,i}) \tag{17}$$

The condenser effectiveness (ϵ) is defined as the ratio between actual heat transfer rate to maximum heat transfer rate:

$$\epsilon = \frac{Q_a}{Q_m} \tag{18}$$

The effectiveness of cross flow heat exchanger with unmixed fluid is a function of the specific heat ratio (C_{\min} / C_{\max}) and the number of transfer units (Incropera and DeWitt, 1990).

For single phase region

$$\epsilon = 1 - \exp \left\{ \frac{NTU^{0.22}}{C_{\min} / C_{\max}} \left[\exp((-C_{\min} / C_{\max}) * NTU^{0.78}) - 1 \right] \right\} \tag{19}$$

For two phase region

$$\epsilon = 1 - \exp(- NTU) \tag{20}$$

Where the number of transfer units is calculated for each region to determine the heat transfer rate. This parameter is defined as follows:

$$NTU = \frac{U A}{C_{\min}} \tag{21}$$

Where $C_{\min} = \min(C_m, C_{um})$, the refrigerant is modeled as mixed fluid and the air is modeled as unmixed fluid

$$C_m = \dot{m}_r C_{p_r} \tag{22}$$

$$C_{um} = \dot{m}_a C_{p_a}$$

The UA value denotes the overall thermal conductance of any region in the condenser in

$W/^{\circ}C$. The overall thermal conductance is computed as:

$$\frac{1}{UA} = \frac{1}{h_r A_{t,i}} + \frac{\delta_t}{k_t A_{t,m}} + \frac{1}{h_{f, A_{t,o}}} + \frac{1}{\eta_o h_a A_o} \quad (23)$$

By neglecting the very small resistances of the tube wall and the thermal contact resistance, the overall thermal conductance reduce to;

$$\frac{1}{UA} = \frac{1}{h_r A_{t,i}} + \frac{1}{\eta_o h_a A_o} \quad (24)$$

In single-phase region (liquid or vapor), the forced convection heat transfer coefficient of the refrigerant side for a smooth tube was determined using the Dittus-Boelter equation (Incropera and DeWitt, 1990)

$$h_{r,s} = 0.023 \cdot Re^{0.8} \cdot Pr^a \frac{k_r}{D_i} \quad (25)$$

For liquid phase: (a=0.3)

$$Re_L = \frac{G \cdot d_i}{\mu_L}, \quad Pr_L = \frac{Cp_L \mu_L}{k_L} \quad (26)$$

For vapor phase(a=0.4)

$$Re_v = \frac{G \cdot d_i}{\mu_v}, \quad Pr_v = \frac{Cp_v \mu_v}{k_v} \quad (27)$$

In the two phase region, the condensation heat transfer coefficient correlations by Shah (1979) was employed. This correlation is calculated as a function of the vapor quality. It can be written as follows:

$$h_{r,t} = h_l \left[(1-x)^{0.8} + \frac{3.8 x^{0.76} (1-x)^{0.04}}{P_{re}^{0.38}} \right] \quad (28)$$

Where the liquid heat transfer coefficient, h_l , is calculated using the Dittus-Boelter equation and P_{re} is the reduced pressure of refrigerant ($P_{re} = P_{sa}/P_{cr}$). Furthermore, the average convection heat transfer coefficient in the condenser and evaporator is obtained by integrating local values over the length of the two phase region. The vapor quality of the

refrigerant is assumed to be linear throughout the length. Therefore, the integration is performed over the range of refrigerant vapor quality. The average condensing heat transfer coefficient, $h_{av,t}$, is thus given by:

$$h_{av,t} = \frac{1}{x_o - x_i} \int_{x_{in}}^{x_{out}} h_{r,t}(x) dx \quad (29)$$

Where x_i and x_o are vapor quality of refrigerant at the inlet and outlet of the condenser ($x_i=1$ and $x_o=0$).

The air side heat transfer coefficient for dry surfaces is based on the work of McQuiston (1981) and is calculated by the correlation :

$$h_{c,a} = \frac{J Cp_a G_m}{Pr^{2/3}} \quad 3000 < Re < 15000 \quad (30)$$

The dry fin efficiency for a thin insulated tip with uniform rectangular section is based on the Schmidt method as described by Incropera and DeWitt (1990).

$$\eta_f = \frac{\tanh(ml)}{ml} \quad (31)$$

The parameters m and l are defined as:

$$m = \sqrt{\frac{2 h_a}{k_f \delta_f}} \quad (32)$$

$$l = r_e \varphi = r_e \left[\left(\frac{r_e}{r_0} - 1 \right) \left[1 + 0.35 \log \left(\frac{r_e}{r_0} \right) \right] \right] \quad (33)$$

Where r_e is equivalent radius, and r_o is the outer radius of the fin. The equivalent radius parameter is given by the equation.

$$\frac{r_e}{r_0} = 1.28 \psi (\beta - 0.2)^{1/2} \quad (34)$$

$$\psi = \frac{S_t}{2r_0} \quad (35)$$

$$\beta = \frac{S_L}{S_t} \quad \beta \geq 1 \quad (36)$$

Where: S_L and S_t are longitudinal and transverse pitch, respectively. S_L is always selected to be greater than or equal to S_t . Finally, the overall heat transfer rate for the entire condenser is the sum of the heat transfer rates for the three regions

$$Q_c = Q_{de} + \sum_{i=1}^n Q_{t,i} + Q_{sb} \quad (37)$$

Where n is number of condensing region segments.

2.3 Adiabatic Capillary Tube Modeling

The capillary tube is a constant area expansion device used widely in small scale air conditioner systems. The refrigerant flow inside the capillary tube can be divided into the single phase and two-phase regions. **Fig.4** shows a schematic diagram of the straight capillary tube connecting the outlet of the condenser and the inlet of the evaporator.

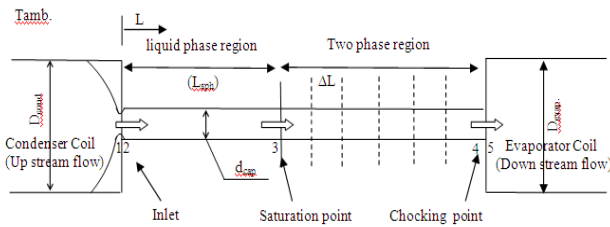


Fig.4 Schematic diagram of a capillary tube

The following assumptions are made:

- 1.The capillary tube operates at steady state.
- 2.Single and two phase flow analysis are considered.
- 3.A subcooled liquid state enters the capillary tube .
- 4.The flow of refrigerant inside the capillary tube is one dimensional, homogenous and adiabatic.
- 5.Changes in kinetic and potential energies are negligible.
- 6.The capillary tube is a straight and horizontal tube with a constant cross-sectional area.

The geometrical parameters and input conditions to the capillary tube model are inner diameter, temperature and pressure of the subcooled liquid refrigerant, and thermophysical properties of refrigerant. Results of the capillary tube model are the pressure and temperature at capillary tube exit and the capillary choking length.

By applying the Bernoulli equation between points 1 and 2, the minor pressure drop at the entrance is calculated by Sinpi boon and Wongwises (2002);

$$P_1 - P_2 = (1 + k) \frac{\rho V^2}{2} \quad (38)$$

Where k is the entrance loss factor. References are not in agreement about its value. The value of $k=0.5$ is used here as given by Chen (2008).

In the single phase region (points 2→3), the pressure at point 2 decreases linearly until the saturation pressure at point 3 according to the following equation (Munson and Young 2010).

$$P_2 - P_3 = f_s \frac{L_{c.s}}{d_{ca}} \frac{\rho V^2}{2} \quad (39)$$

By applying the steady flow energy equation for the single phase liquid region in the capillary tube with negligible work and heat exchange, we get:

$$H_2 = H_3 = H_{sc} \quad (40)$$

Applying the steady flow energy equation for each element lying in the two phase region, between sections 3 and 4:

$$H_3 + \frac{V_3^2}{2} = H_f + x H_{fg} + \frac{G^2}{2} (v_f + x.v_{fg})^2 \quad (41)$$

Eq.41 is quadratic in the quality x . It is given with other details and the choking length by Sukkarin and Somchai, 2011.

2.4 Modeling of a Direct Expansion Evaporator

The analysis for the evaporator model is similar to that of the condenser, but is assumed to contain two heat transfer regions on the refrigerant

side, namely a two phase evaporating region and a single phase superheated region. In addition, the air side cooling region is divided into two sections which are dry and wet. **Fig.5** shows the refrigerant flow through the evaporator.

The following assumptions are made for the evaporator model:

1. Fin edges are adiabatic
2. Fin efficiency is assumed to be 90%
3. The degree of superheating at the evaporator is assumed to be 6 °C.
4. Dehumidification occurs on the air side at the entrance of two phase region.
5. Heat transfer and pressure drop effects due to bends are neglected.

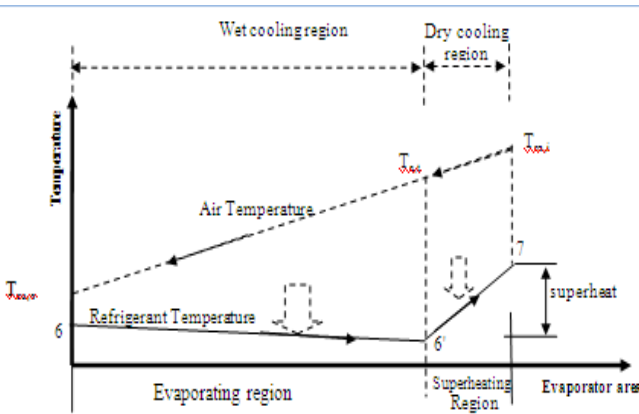


Fig.5 Temperature diagram in an evaporator coil

The heat gain by the refrigerant side in the two phase and superheated regions are given by the formulae ;

$$Q_{e,t} = \dot{m}_r (H_6 - H_6) = \varepsilon_t^* C_{\min,t} (T_{a,t} - T_6) \quad (42)$$

$$Q_{e,sp} = \dot{m}_r (H_7 - H_6) = \varepsilon_{e,sp} C_{\min} (T_{ro,i} - T_6) \quad (43)$$

Where H_6 , H_7 and H_6 are refrigerant enthalpies at the locations in **Fig.5**. The modified heat

exchanger effectiveness ε_t^* is given by Harms et al (2002) as;

$$\varepsilon_t^* = 1 - \exp \left(-\frac{UA^*}{m_a C_{p_a}} \right) \quad (44)$$

Where UA^* is the overall heat transfer coefficient for the wet cooling region.

The overall thermal conductance of the wet region of the evaporator coil is computed as

$$\frac{1}{UA^*} = \frac{1}{h_r A_{t,in}} + \frac{1}{h_l A_0} + \frac{1}{h_{a,w} \eta_{o,w} A_0} \quad (45)$$

McQuiston and Tree (1973) assumed a linear relationship between the humidity ratio of the saturated air at the wet surface, and the surface temperature. These parameters are determined as follows:

$$h_l = \frac{k_{wa}}{\delta_{wa}} \quad (46)$$

$$h_{a,w} = h_{a,dry} \left\{ 1 + \frac{H_{fg,w} (w_a - w_w)}{L_e C_{p_a} (T_a - T_w)} \right\} \quad (47)$$

$$H_{fg,w} = \left(-2 * 10^{-5} T_w^3 + 0.0012 T_w^2 - 2.3804 T_w + 2501.6 \right) * 10^3 \quad (48)$$

The moist air properties are obtained using relations given by Joudi,1991.

As in the condenser model, the Dittus-Boelter equation is used to compute the refrigerant side heat transfer coefficient in the single phase region:

$$h_{r,s} = 0.023 . \text{Re}^{0.8} . \text{Pr}^{0.4} \frac{k_r}{D_i} \quad (25)$$

Whereas, the evaporating heat transfer coefficient in the two-phase region ($h_{r,t}$) is calculated as (Domanski and David, 1985) ;

$$h_{r,t} = 3.22 . X_t^{-0.3} h_{r,s} \quad (49)$$

The above correlation is applicable for annular flow at qualities from 10 percent to 90 percent.

The forced convection heat transfer coefficient on the air side of flat finned tube heat exchangers ($h_{a,dry}$) is calculated by the correlation proposed by Briggs and Yong, 1962.

$$h_{a,dry} = 0.134 \frac{k_a}{D_0} Re_a^{0.681} Pr_a^{0.333} \left(\frac{Z}{Y}\right)^{0.2} \left(\frac{Z}{t}\right)^{0.1134} \quad (50)$$

The evaporator cooling capacity is the sum of the combination of heat gains by the refrigerant side in the two phase and superheated regions and can be expressed as:

$$Q_e = \sum_{i=1}^n Q_{e,i} + Q_{e,sp} \quad (51)$$

2.5 System Pressure Drop

Pressure drop in the system consist of pressure drops in the main components of the system and connecting pipes. Conventional equations are used with full details given by Al-Amir 2013.

3. SOLUTION PROCEDURE

The Engineering Equation Solver (EES) software is used in this work for computer programming. The computer program of the actual cycle is more complex when compared to the ideal cycle program and consists of a main program and a number of procedures. These procedures are coupled with the main program by call commands. The main program contains system equations and call statements for all the preceding procedures. Basic inputs are required to the main program to simulate the actual vapor refrigeration cycle performance. These inputs are the physical dimensions of the components and operating conditions for cycle. The output parameters of the system simulation model are the cycle state points, cooling capacity, heat rejection from the condenser, refrigerant pressure drops, consumed power, and the coefficient of performance. To plot the steady state characteristic performance of the actual refrigeration cycle on a p-h diagram, pressure and enthalpy data are taken from the simulation results.

For each refrigerant, five different settings of outdoor air temperature into the condenser were considered. The EES software is used to plot data on a p-h diagram.

4. EXPERIMENTAL WORK

The experimental test rig is shown in **Fig. 6**.

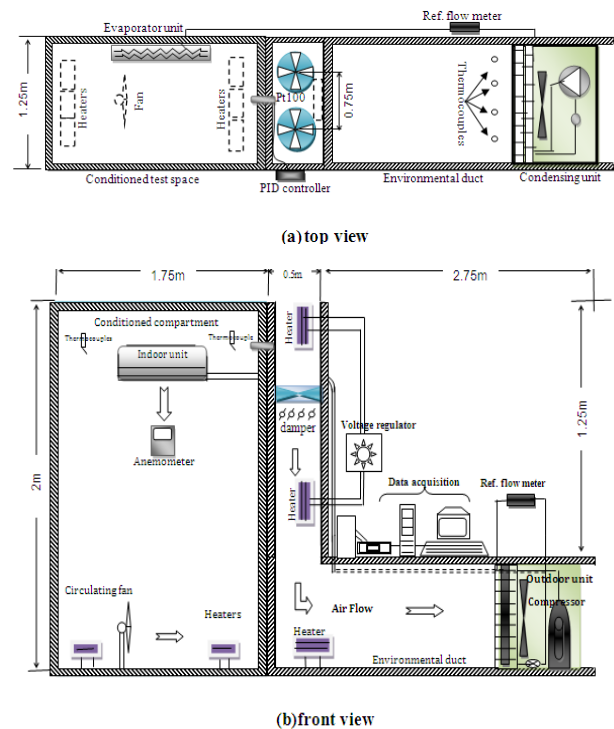


Fig.6 A schematic diagram of the experimental test rig with dimension of conditioned compartment and environmental duct a)top view b) front view

It consists of four main parts which are the refrigeration system, the psychrometric apparatus, measuring instrumentation, and auxiliary systems. Split type air conditioners with a 2 TR nominal cooling capacity model EL-26ITERH manufactured by Denka company were tested experimentally. This system required to replace the compressor for R410A refrigerant due to its higher operating pressures. The psychrometric apparatus consists of two sections, which are the indoor conditioned compartment and the outdoor environmental duct. These sections were locally constructed and their conditions were maintained

according to the ASHRAE standard 37-2009 for testing unitary air conditioners and heat pumps. The dry and wet bulb air temperatures for the interior are 27 °C/19 °C and outdoor ambient are 35 °C/24 °C. The evaporator unit was mounted at a height of 1.75 m. Six electric heaters, 1200 W each, were placed inside the condition compartment for the heat load. They are controlled by a Solid State Relay (SSR) to maintain the air temperature inside the compartment at 25 °C throughout the test period. The environmental duct has an L shape and includes two circulation fans with dampers, which drive the air through the thermally insulated environmental duct. Three electric resistance heaters, 1200 W each, are located inside the duct for controlling the temperature of the air across the condensing unit. All the components such as system units, fans, electric heaters and voltage regulator are connected to a power supply. A sample of systematic test runs is summarized in Table 1.

Table 1 Experimental runs at optimum charge under various outdoor air temperature

The instrumentation required for testing are divided into refrigerant and air sides. Refrigerant side measurements include the thermocouples type-K with a range of -50 to 250 °C and an accuracy of ± (0.4 % + 0.5 °C), pressure transducers with a range of 0-10 bar or 0-40 bar and an accuracy of ±1% of full scale, turbine flow meter with a range of 0.02-1.2 m³/h and an accuracy of ±0.58 of the reading. Whereas, air side measurements include thermocouples type-T with a range of -270 to 400 °C and an accuracy of ± 0.3 °C, and collection vane type anemometer with a range of 0.4 - 30 m/s and an accuracy of ± 3 % full scale. All measurements were calibrated before their use.

5. RESULTS AND DISCUSSION

Fig.7 shows influence of outdoor air temperature on the compressor discharge temperature. Clearly, increasing the outdoor air temperatures increases the compressor discharge temperature. It is noted from the same figure that discharge temperature of the R22 is higher by about

21-23°C than that of R290 at outdoor temperature ranging from 35 °C to 55 °C.

Fig.8 shows the effects of outdoor air temperature on power consumption of compressor when the system operates in the cooling mode. The compressor power consumption increases with increasing outdoor air temperature from 35 °C to 55 °C with a constant 25 °C inside the conditioned compartment. This is because the compressor power is affected by two factors, the refrigerant mass flow rate and the compression ratio. The power consumption increased from 2.365 kW to 2.84 kW for R22, 2.04 kW to 2.65 kW for R290, 2.47 kW to 2.93 kW for R407C, 2.74 kW to 3.32 kW for R410A for the same outdoor temperature range. Also, the power consumption increases with increased outdoor air temperature due to the rise in the temperature difference (lift) between the environmental duct and conditioned compartment.

The system has high cooling capacities at the standard rating conditions (35 °C outdoor air temperature), but lose capacity as the outdoor air

Ref. Type	Charge Level(gram)	No. of Run	Optimum Charge(g)	Outdoor Temp(C)	No. of Run
R22	1500	2	R22 (2000g)	35	2
	1600	2		40	2
	1700	2			
	1800	2		45	2
	1900	2			
	2000	2		50	2
	2100	2			
	2200	2		55	2
2300	2				
R290	200	2	R290 (900 g)	35	2
	300	2		40	2
	400	2			
	500	2		45	2
	600	2			
	700	2		50	2
	800	2			
	900	2		55	2
	1000	2			
	1100	2			
R407C	1500	2	R407C (1900 g)	35	2
	1600	2		40	2
	1700	2			
	1800	2		45	2
	1900	2			
	2000	2		50	2
	2100	2			
	2200	2		55	2
2300	2				
R410A	1800	2	R410A (2800 g)	35	2
	2000	2		40	2
	2200	2			
	2400	2		45	2
	2600	2			
	2800	2		50	2
	3000	2			
	3200	2		55	2

temperature increases as shown in **Fig.9** . The

cooling capacity of R410A has a higher value, at the standard test condition, than the other refrigerants. This is because of the high volumetric refrigerating capacity, which is defined as the cooling capacity per unit vapor volume at the exit of the evaporator in kJ/m^3 . Moreover, the mass flow rate of R410A is higher than the other refrigerants at this condition. When the outdoor air temperature increases to 55°C , the cooling capacity of R410A drops faster than the other refrigerants because of its low critical temperature (72.5°C). Theoretical results for 2 TR system using R410A is higher by about 3.82 % than that of R22 while it is lower for the alternative refrigerants R407C and R290 by about 1.66 % and 4.63 % than that of R22, respectively.

Fig.10 indicates that the lower the outdoor air temperature, the higher is the COP. As the outdoor temperature increases, the COP values decrease for all refrigerants. With increasing outdoor temperature, the COP of system charged with R410A drops much more than that of the same system charged with other refrigerants. Which means, the COP of R410A system is more sensitive to changes in outdoor temperature. On the other hand, the system charged with R290 has the highest COP among the selected refrigerants at standard conditions. The COP of R407C seems to be similar to R22, as expected. At maximum outdoor air temperature (55°C), the coefficient of performance is maximum for R290 and minimum for R410A.

6. VALIDATION OF THE THEORETICAL MODEL WITH EXPERIMENTAL DATA

The normal way of validation of a theoretical model is by comparison with experimental results at the same operating conditions. The deviations between the two results are calculated by the following formulas;

$$\text{Relative deviation } (x \%) = \frac{(x_{\text{theoretical}} - x_{\text{experimental}})}{x_{\text{experimental}}} \times 100 \quad (52)$$

$$\text{Average deviation. } (x_{\text{av}} \%) = \frac{1}{n} \sum_{i=1}^n \left[\frac{(x_{i,\text{theoretical}} - x_{i,\text{experimental}})}{x_{i,\text{experimental}}} \times 100 \right] \dots\dots(53)$$

Fig.11 shows the comparison between calculated and measured compressor discharge temperatures for outdoor air temperatures of 35°C , 40°C , 45°C , 50°C and 55°C . **Fig.(11)** include 40 experimental data points, 10 data points for each refrigerant. The compressor discharge temperature calculations agree well with experimental measurements. All the points are within -3.198% and +4.4% .

A comparison of calculated and measured compressor work with different outdoor air temperatures is shown in **Fig.12**. The measured results, lie within a maximum deviation of 6.92% and a minimum deviation of -4.07 % .

Good agreement is observed between the calculated and measured cooling capacity at different outdoor air temperatures as shown in **Fig.13**. The maximum deviation in the system is +11.7%. All the theoretical values are higher than the experimental values for all four refrigerants.

The calculations of the coefficient of performance for the actual cycle lead to good results, as illustrated in **Fig. 14**. For R22, the average deviation in the coefficient of performance was 3.68% and minimum deviation of -3.38%. The theoretical predictions for COP values are higher than the experimental values for the actual cycle.

The actual cycle diagrams (**Figs. 15 to 18**) clearly show the effect of outdoor temperature at a relatively constant evaporator temperature. Pressure drops across suction line and discharge valve of compressor are very clear and the minor pressure drops inside the condenser and evaporator are obvious. These characteristics are, of course, not present in the assumptions for the ideal cycles.

7. CONCLUSIONS

1. At standard rating conditions, the cooling capacity for R410A was highest among the investigated refrigerants.
2. The compressor discharge temperature increase with increasing outdoor air temperatures. R22 refrigerant has higher discharge temperature than the other refrigerants.

3. The system charged with R290 has the best COP than the other refrigerants.
4. The comparison shows that the power consumption of R410A and R407C are higher by about 15.8-16.9% and 4.4-3.17%, respectively and R290 lower by about 13.7-6.7% as compared to R22 under same operating conditions. Test results demonstrate that R290 is a good alternative to replace R22 in air conditioners from the standpoint of energy efficiency.
5. The results also show that the COP values decrease for all investigated refrigerants, as the outdoor temperature increases. The COP for 2 TR system using R410A is found to be the lowest among the four refrigerants at high outdoor air temperature. Therefore, R410A is not a good choice for air conditioner in high outdoor air temperature.

REFERENCES

- Al-Amir Q. R., 2013," Experimental assessment and numerical simulation of the performance of small scale air-conditioning systems using alternative refrigerants to R-22" University of Baghdad, PhD thesis.
- ASHRAE. 2009, ANSI/ASHRAE 37-2009," Methods of Testing for Rating Electrically Driven Unitary Air Conditioning and Heat Pump Equipment", American Society of Heating, Refrigeration, and Air-Conditioning Engineers, Inc.
- ASHRAE Handbook of Fundamental, 2010, American society for Heating, Refrigeration and Air Conditioning Engineers, Inc., New York, Chapter 6.
- Blanco D., Nagano K., Morimoto M., 2012" Steady state vapor compression refrigeration cycle simulation for a monovalent inverter-driven water-to-water heat pump with a desuperheater for low energy houses" International journal of refrigeration, 35, 1833- 1847.
- Briggs, D.E. and Yong, 1962," Convection heat transfer and pressure drop of air flowing across triangular pitch banks of finned tubes", 5th AICHE/ASME.
- Cabello R., Navarro J., Torrella E., 2005, " Simplified steady-state modelling of a single stage vapor compression plant. Model development and validation" Applied Thermal Engineering 25, 1740–1752.
- Chang Y., Wang C., 1997, "A Generalized Heat Transfer Correlation for Louver Fin Geometry", *International Journal of Heat and Mass Transfer*, Vol.40, pp. 533-544.
- Chen W., 2008," A comparative study on the performance and environmental characteristics of R-410A and R-22 residential air conditioners", Applied Thermal Engineering , Vol. 28, 1-7.
- Cho I. S and Jung J.Y., 2010," Lubrication characteristics of a rotary compressor used for refrigeration and air-conditioning systems ", Journal of Mechanical Science and Technology 24 (4), 851-856.
- Ding G., Hu H., Huang X., Deng B., Gao Y., 2009," Experimental investigation and correlation of two-phase frictional pressure drop of R410A–oil mixture flow boiling in a 5mm micro fin tube" International Journal of Refrigeration. 32, ,150 –161.
- Ding G.L., Zhang C.L., 2001, "Simulation and Optimization of Refrigeration and Air Conditioning Appliances, Science Press, Beijing. Quoted by Zhou (2010).
- Domanski, P.A., and David A. D., 1985," Simulation of a Heat Pump Operating with a Non azeotropic Mixture, ASHRAE Technical Data Bulletin" Advances in Non azeotropic Mixture Refrigerants for Heat Pumps, Vol.1, No.9, pp. 81, ASHRAE, Inc., Atlanta, GA.
- Domanski P. A., Yashar D., Kim M., 2005, " Performance of a finned-tube evaporator optimized for different refrigerants and its effect on system efficiency ", International Journal of Refrigeration 28, 820–827.
- Duprez, M.E., Dumont E., Frere M., 2007," Modeling of reciprocating and scroll compressors", International Journal of Refrigeration, 30, 5, 873-886.
- Fisher S.K., Rice C.K., 1983, "A steady-state computer design model for air to air heat pumps", Oak Ridge National Laboratory, Oak Ridge, Tennessee, U.S.A.
- Harms T. M., Braun J. E., and Groll E. A., 2002 "The Impact Of Modeling Complexity And Two-Phase Flow Parameters On The Accuracy Of System Modeling For Unitary Air Conditioners" , International Refrigeration and Air Conditioning Conference. Paper 569.



Incropera F., DeWitt D., 1990, "Fundamentals of Heat and Mass Transfer", third ed., John Wiley & Sons Inc., New Jersey, USA.

Jin H., and Spitler J.D., 2002. "A Parameter Estimation Based Model of Water-To-Water Heat Pumps for use in Energy Calculation Programs", ASHRAE Transactions, 108(1), pp. 3-17.

خالد احمد الجودي، 1991. مبادئ هندسة تكييف الهواء و التثليج، الطبعة الثانية، كلية الهندسة، جامعة البصرة.

Kim M.H., Bullard C.W., 2001, " A Simple Approach to Performance Analysis of Alternative Refrigerant Rolling Piston Type Rotary Compressors", MSc thesis, University of Illinois at Urbana Champaign.

Klein S.A., 2006, Engineering Equation Solver commercial version V8.914 .

McQuiston F. C., 1981, "Finned tube heat exchangers: state of the art for the air side", ASHRAE Trans., Vol.87, Part1, 1077-1085.

McQuiston F. C., Tree D. R., 1973, "Optimum space envelopes of the finned tube heat transfer surface," ASHAE Transactions, Vol.79, Pt. 2.

Munson B. R., Young D. F., 2010, " Fundamentals of Fluid Mechanics" Fourth edition, John Wiley & Sons. Inc. USA.

Rice C.K., Fisher S.K., Jackson W.L., Ellison R.D.,1981, "Design optimization and the limits of steady state heating efficiency for conventional single speed air source heat pumps", Oak Ridge National Laboratory, Oak Ridge, Tennessee ,U.S.A.

Richardson D. H., Aute V., Winkler J., and Radermacher, R. , 2004, " Numerical Challenges in Simulation of a Generalized Vapor Compression Refrigeration System." 2004 International Refrigeration and Air Conditioning Conference. Purdue University.

Sakaino K., Muramatsu S., Shida S., Ohinata O., 1984, " Some Approaches Towards a High Efficient Rotary Compressor, " International Compressor Engineering Conference, Purdue University.

Shah MM. , 1979, "A general correlation for heat transfer during lm condensation inside pipes". International Journal Heat and Mass Transfer, 22:547-56.

Sinpiboon J. , Wongwises S., 2002," Numerical investigation of refrigerant flow through non-adiabatic

capillary tubes" Applied Thermal Engineering , 22, 2015–2032.

Spatz M. W., 2004, "Replacement for HCFC-22 in air conditioning and heat pump system".

Sukkarin C., Somchai W., 2011," A comparison of flow characteristics of refrigerants flowing through adiabatic straight and helical capillary tubes" International Communications in Heat and Mass Transfer 38, 398–404.

Techarungpaisan P., Theerakulpisut S., Priprem S., 2007, "Modeling of a split type air conditioner with integrated water heater", Energy Conversion Management, 48, 1222-1237.

Wakabayashi H., Yuuda J., Aizawa T., Yamamura M., 1982," Analysis of Performance in a Rotary Compressor" International Compressor Engineering Conference, Paper 385.

Wang S. K. , 2000, " Handbook of air conditioning and refrigeration" Second Edition, chapter 10 page 26.

Winandy E., Saavedra O. C. , Lebrun J., 2002, "Simplified modelling of an open-type reciprocating compressor" Int. J. Therm. Sci. 41, 183–192.

Winkler J. M. ,2009," Development of a component based simulation tool for the steady state and transient analysis of vapor compression systems", PhD Thesis, University of Maryland, College Park

NOMENCLATURE

A	Area (m^2)
C_p	Specific heat at constant pressure ($J/kg.^{\circ}C$)
C_v	Specific heat at constant volume ($J/kg.^{\circ}C$)
d_{ca}	Capillary tube diameter(m)
D_h	Hydraulic diameter (m)
f_s	Friction factor
G	Mass flux ($kg/s.m^2$)
h	heat transfer coefficient ($W/m^2.^{\circ}C$)
H	Enthalpy(kJ/kg)
J	Colburn J factor
k	Thermal conductivity ($W/m.K$)
K	Entrance loss factor
k_t	thermal conductivity of wall tube ($W/m.K$)
Le	Lewis number
m	mass flow rate(kg/s)
n	Polytropic index

n_f	number of fins
n_{ro}	number of rows.
n_{tu}	number of tube
N	Number of cycles per minute(N=3600)
Nu	Nusselt number
P	Pressure (kPa)
Pr	Prandtl number
P_{re}	Reduce pressure
Q	Heat (kW)
Re	Reynolds number
S_L	Longitudinal pitch (m)
S_t	Tangential pitch (m)
T	Temperature (K)
U	Overall heat transfer coefficient (W/m^2K)
v_l	Specific volume at the comp. suc. (m^3/kg)
V_d	Displacement Volume of the compressor (m^3)
W	Compressor power (kW)
x	Quality
X_{tt}	Lockhart Martinelli parameter

r	refrigerant
s	suction
S	Shell
t	Tangential
v	vapor

ABBREVIATIONS

COP	Coefficient Of Performance
EES	Engineering Equation Solver
GWP	Global Warming Potential
HC	Hydrocarbon
HCFC	Hydro chlorofluorecarbon
HFC	Hydro fluorocarbon
PID	Proportional Integral Derivative
TR	Tone of Refrigeration

Greek Symbols

γ	Adiabatic index
ε	Effectiveness
ε_v	Void fraction
ΔP_d	Pressure drop across the discharge valve
η_0	Efficiency
μ	Dynamic viscosity ($kg/m \cdot s$)
ν	Kinematic viscosity(m^2/s)
ρ	Density (kg/m^3)
Φ_{Lt}	Two phase liquid multipliers
Φ_{vt}	Two phase vapor multipliers
δ_f	Fin thickness(mm)
δ_t	Wall thickness of the tube ($\delta_t=0.5mm$).
σ	Surface tension (N/m)
Δh	Enthalpy change (kJ/kg)
X_{tt}	Lockhart Martinelli parameter

SUBSCRIPTS

c	condenser
co	compressor
d	discharge
e	evaporator
i	input
l	liquid

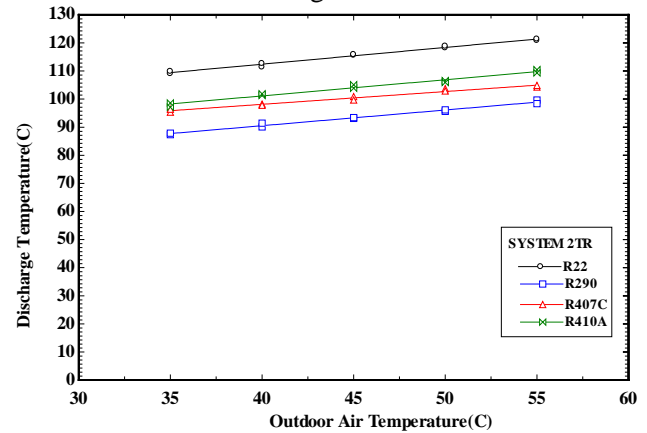


Fig. 7 The effect of the outdoor air temperatures on discharge temperature.

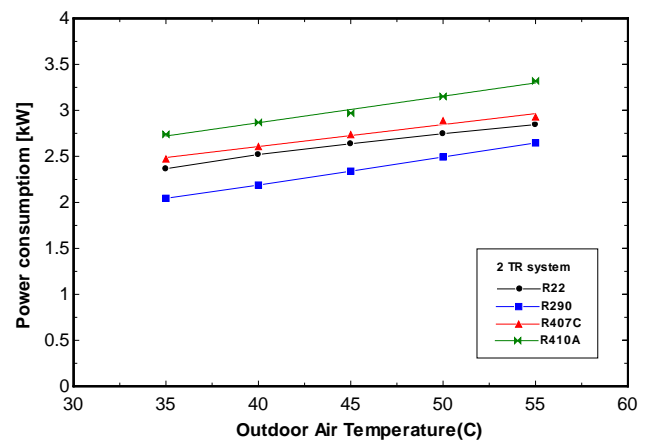


Fig. 8 The effect of the outdoor air temperatures on compressor power consumption

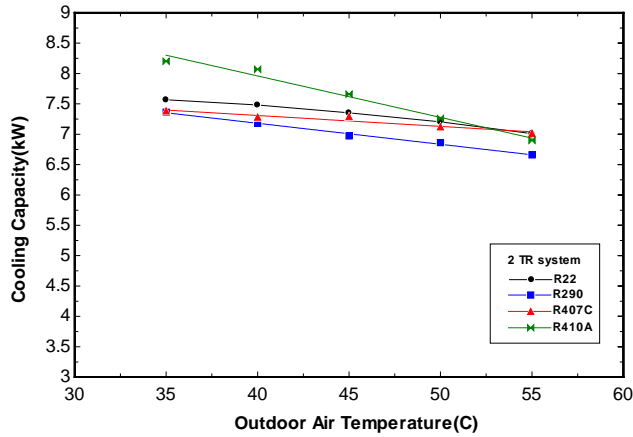


Fig. 9 The effect of the outdoor air temperatures on evaporator cooling capacity .

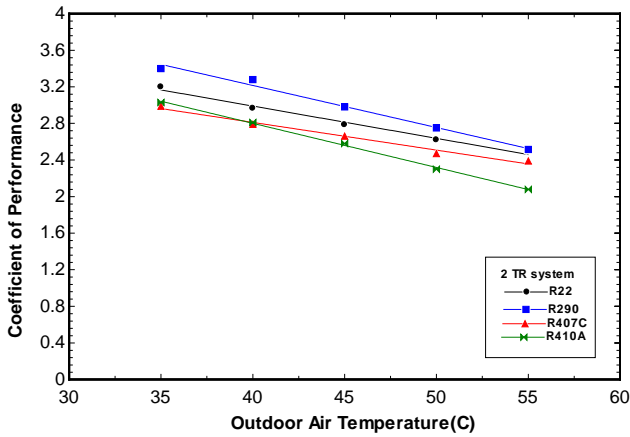


Fig. 10 The effect of the outdoor air temperatures on COP of system.

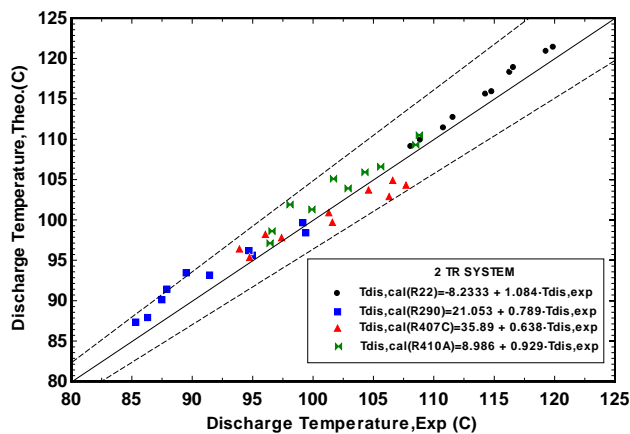


Fig.11 Comparison between theoretical and experimental compressor discharge temperatures system working with R22 and its alternative.

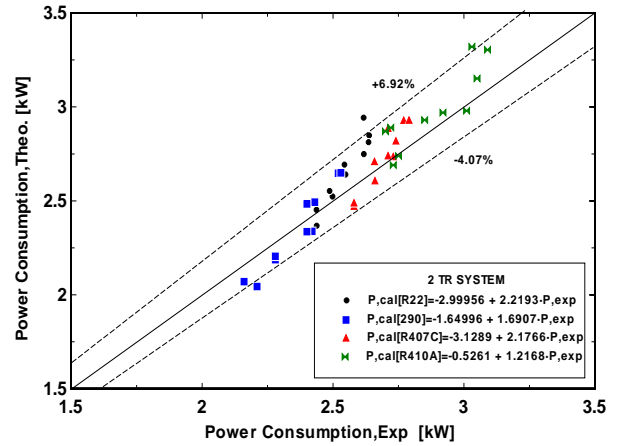


Fig.12 Comparison between calculated and measured compressor power consumption for system working with R22 and its alternative.

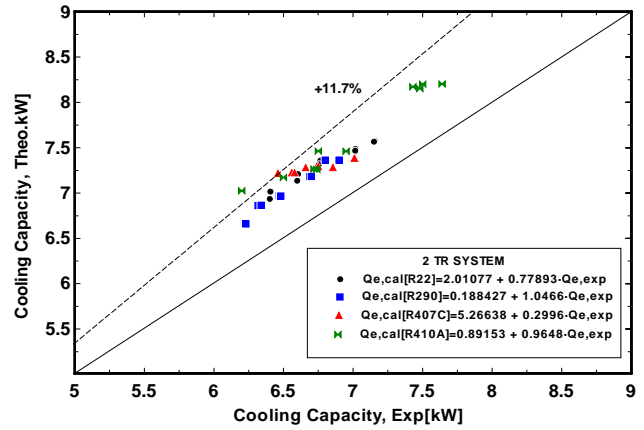


Fig.13 Comparison between theoretical and experimental cooling capacity for system working with R22 and its alternative.

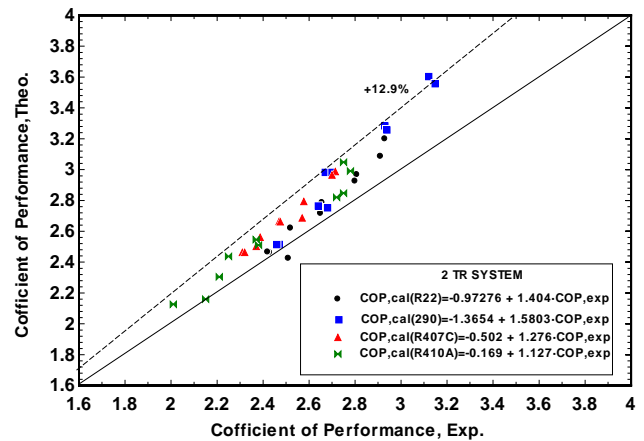


Fig.14 Comparison between theoretical and experimental coefficient of performance for system working with R22 and its alternative

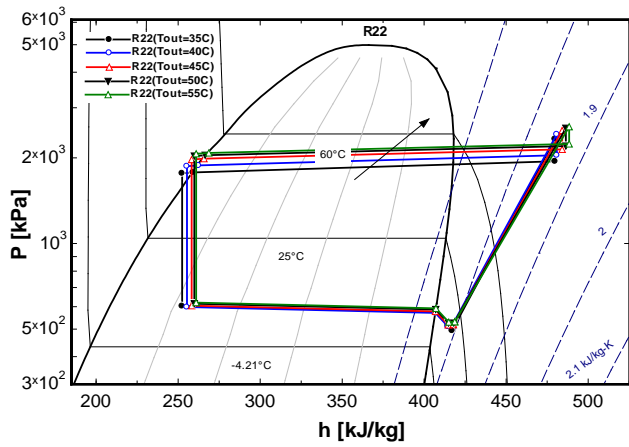


Fig.15 Pressure-enthalpy diagram of actual cycle for R22 under different outdoor air temperatures

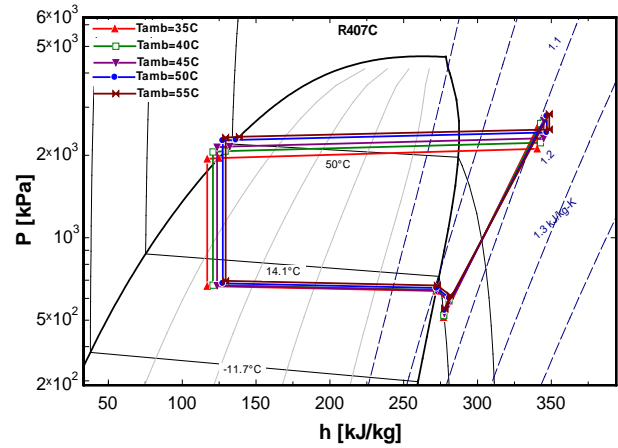


Fig. 17 Pressure-enthalpy diagram of actual cycle for R407C under different outdoor air temperatures

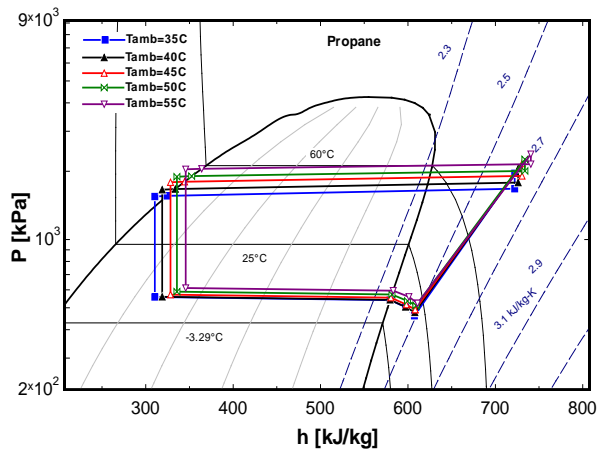


Fig. 16 Pressure-enthalpy diagram of actual cycle for R290 under different outdoor air temperatures

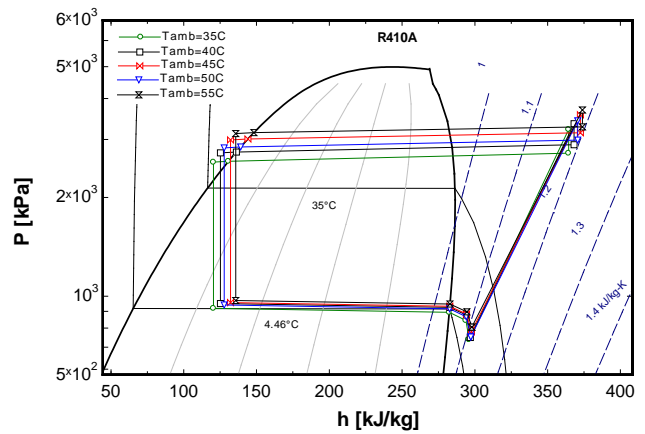


Fig.18 Pressure-enthalpy diagram of actual cycle for R22 under different outdoor air temperatures